

The Ensemble Kalman Inversion Race

Rebecca Gjini¹, Matthias Morzfeld¹, Oliver R.A. Dunbar², and Tapio Schneider²

¹Cecil H. and Ida M. Green Institute of Geophysics and Planetary Physics, Scripps Institution of Oceanography, University of California, San Diego, CA
²California Institute of Technology, Pasadena, CA

Key Points:

- Ensemble Kalman methods effectively calibrate climate model parameters from noisy, time-averaged data, where derivative-based methods fail
- No single method wins all “races,” but Tikhonov ensemble Kalman inversion and ensemble transform Kalman inversion are most robust
- Unscented Kalman inversion is efficient for low-dimensional problems with good priors

Corresponding author: Rebecca Gjini, rgjini@ucsd.edu

Abstract

Ensemble Kalman methods were initially developed to solve nonlinear data assimilation problems in oceanography, but are now popular in applications far beyond their original use cases. Of particular interest is climate model calibration. As hybrid physics and machine-learning models evolve, the number of parameters and complexity of parameterizations in climate models will continue to grow. Thus, robust calibration of these parameters plays an increasingly important role. We focus on learning climate model parameters from minimizing the misfit between modeled and observed climate statistics in an idealized setting. Ensemble Kalman methods are a natural choice for this problem because they are derivative-free, scalable to high dimensions, and robust to noise caused by statistical observations. Given the many variants of ensemble methods proposed, an important question is: *Which ensemble Kalman method should be used for climate model calibration?* To answer this question, we perform systematic numerical experiments to explore the relative computational efficiencies of several ensemble Kalman methods. The numerical experiments involve statistical observations of Lorenz-type models of increasing complexity, frequently used to represent simplified atmospheric systems, and some feature neural network parameterizations. For each test problem, several ensemble Kalman methods and a derivative-based method “race” to reach a specified accuracy, and we measure the computational cost required to achieve the desired accuracy. We investigate how prior information and the parameter or data dimensions play a role in choosing the ensemble method variant. The derivative-based method consistently fails to complete the race because it does not adaptively handle the noisy loss landscape.

Plain Language Summary

The resolution of global climate models is too coarse to resolve many important but small-scale processes, such as clouds. Parameterization schemes are used to represent these unresolved atmospheric processes, including machine learned parameterizations. These parameterizations contain many unknown parameters. A promising approach to improving models and their parameterizations is to calibrate them by matching model statistics (not exact trajectories) to observations. Ensemble Kalman methods are promising for this task because they are derivative-free, scalable, and robust to the noisy data generated by aggregating climate statistics. Since many variants exist, we investigate which ensemble method is most efficient for this calibration problem. We set up systematic numerical experiments, “racing” several methods to see which reaches a specified accuracy at the lowest computational cost. Our findings reveal guidelines for the efficient use of ensemble methods for learning unknowns within climate models.

1 Introduction

Global climate models (GCMs) are important tools for making climate projections. To make projections, GCMs evolve a coarsely discretized state of the Earth system, often over several decades, and statistical projections are inferred from these trajectories. GCMs have two components: dynamics, defined by the laws of motion resolvable on the discretization grid-scale, and parameterizations, representing the effect of unresolved sub-grid processes, e.g., cloud microphysics, convection, and turbulence. Depending on the current understanding of the processes being represented, parameterizations may rely on specified functional forms, sets of auxiliary differential equations, or they may need to be learned, e.g., with machine-learning (ML). To learn unknown parameters or functionals, GCMs can be calibrated to observations of Earth’s climate (Schneider, Lan, et al., 2017; Schneider et al., 2023).

Calibration of GCM parameterizations by matching trajectories is challenging as chaos drives an exponential divergence of trajectories with non-identical initial conditions; it begins to dominate misfit to data at relatively short lead-times of about two weeks.

Even sophisticated techniques that calibrate states and parameters jointly with separate ensembles have seen limited success (e.g., Santitissadeekorn and Jones (2015) and references therein). A more recent and promising approach to GCM calibration involves minimizing a loss defined by the misfit of modeled and observed climate statistics (Schneider et al., 2024; Schneider, Lan, et al., 2017). A statistics-based loss function has the advantage that initial conditions are largely irrelevant (forgotten) and need not be computed; there is no chaotic divergence of statistical quantities, and the loss becomes primarily a function of the parameters. The disadvantage is that the chaotic variability of the climate system instead induces noise in the loss function (Dunbar et al., 2021; Cleary et al., 2021). The noisy loss landscape and the lack of adjoints or automatic differentiation available for GCMs render the minimization of the loss via traditional, derivative-based optimization difficult. The noise level of statistical aggregates decreases slowly with accumulation time, and so even if gradients were available, a sufficient noise reduction for successful application of derivative-based approaches requires prohibitively long integration times (Cleary et al., 2021). Even with relatively short accumulation times (e.g., months to seasons), computational efficiency of algorithms for minimizing the loss is paramount, given the large computational expense of GCM integrations.

A further challenge is that the GCM calibration problem is high-dimensional: For recent ML parameterizations, the unknowns are weights and biases of a (deep) neural network and could number hundreds or many more. Therefore, it is crucial to determine which optimization algorithms can tackle this high-dimensional and computationally demanding task efficiently, and without sacrificing accuracy.

One candidate class of algorithms with potential for GCM calibration goes by the name *iterative ensemble Kalman methods*, which aim to approximate a Bayesian posterior distribution through an ensemble. The first ensemble Kalman methods were originally developed for solving nonlinear data assimilation problems (state estimation) in oceanography, with the most common being the ensemble Kalman filter (EnKF, Evensen (1994, 2009)). Over the years, many iterative versions of the EnKF have been created and applied for solving nonlinear inverse problems (parameter estimation). Examples of iterative ensemble methods include randomized maximum likelihood (EnRML) (Gu & Oliver, 2007), iterative ensemble smoothers/filters (IES/IEKF Chen and Oliver (2012, 2013)), the ensemble smoother with multiple data assimilation (ESMDA, Emerick and Reynolds (2013, 2012)), and the iterative ensemble Kalman smoother (IEnKS, Bocquet and Sakov (2014)). Connections between various iterative ensemble methods were reported by Evensen (2018). Iterative ensemble methods are commonly used to match instances of sequential time-series data in reservoir engineering, numerical weather prediction (NWP), and physical oceanography (to name a few applications); however, they have not been tested on noisy loss functions, defined by inverting statistical data.

Another class of ensemble-based algorithms goes by the name of *ensemble Kalman inversion* (EKI, Iglesias et al. (2013)). These algorithms are designed to optimize a loss function by collapsing an ensemble onto the minimizer of the loss. The collapse of the ensemble distinguishes EKI from the iterative ensemble Kalman methods described above; it renders EKI methods unsuitable for uncertainty quantification. Variants of EKI algorithms include Tikhonov regularized EKI (TEKI, Chada et al. (2020)), ensemble transform Kalman inversion (ETKI, Huang, Huang, et al. (2022)), and unscented Kalman inversion (UKI, Huang, Schneider, and Stuart (2022)). Examples of EKI handling the noisy loss functions we expect to encounter during GCM calibration are shown in Cleary et al. (2021), and some variants have already been applied successfully to climate science problems (Bieli et al., 2022; Schneider et al., 2020; Lopez-Gomez et al., 2022; Christopoulos et al., 2024; Deck et al., 2025). Many EKI variants are also easily accessible in the Julia toolbox `EnsembleKalmanProcesses.jl` (Dunbar et al., 2022).

An important clarification is that ensemble Kalman methods are not restricted to Gaussian priors and likelihoods, or quadratic loss functions. These methods make use

of ensemble Kalman updates that are derived from linear and Gaussian problems (Gaussian priors and likelihoods), but the overall result is *not* a Gaussian or quadratic approximation. An EnKF ensemble, for example, in general does not have a Gaussian distribution, and EKI makes use of local statistical linearization in much the same way as Gauss-Newton methods use iterative, local linearization for the solution of nonlinear problems. Our numerical experiments clearly demonstrate that EKI can successfully minimize complex loss landscapes that need not be quadratic.

Given the many variants of EKI and iterative ensemble methods, an important question one should ask is: *Which ensemble method should I use to estimate parameters from time-averaged data and chaotic dynamics?* In this paper, we contribute to finding an answer to this question by determining the relative computational efficiencies of several ensemble methods in a set of systematic and idealized prototype experiments. We focus on ensemble-based optimization and test diverse variants of EKI (TEKI, ETKI, UKI), but we also consider IEKF as a representative of an iterative ensemble method. Other iterative ensemble methods, e.g., ESMDA, require more tuning, e.g., for the number of iterations, which makes systematic numerical experiments difficult to perform. We note future work should look closer at iterative ensemble methods, particle samplers (such as the ensemble Kalman sampler (Garbuno-Inigo, Hoffmann, et al., 2020; Garbuno-Inigo, Nüsken, & Reich, 2020)), and particle-based accelerations (such as Calibrate, Emulate, Sample (Cleary et al., 2021; Dunbar et al., 2021)) as parametric uncertainty quantification is vitally relevant for making forecasts with a GCM.

For each numerical experiment we define chaotic dynamics using different Lorenz-type models (Lorenz, 1963, 1995) and then use ensemble methods to minimize a loss function defined by the misfit between modeled and observed statistics. Each ensemble method must reach a specified accuracy, and we evaluate performance of this race by the number of forward model runs needed to reach that accuracy (since the forward model runs, rather than the ensemble updates, dominate the computational cost in our applications of interest). For each ensemble method, we first determine an optimal ensemble size to maximize computational efficiency (with the exception of UKI, for which the ensemble size is a function of the number of unknowns). To highlight the difficulties derivative-based optimization encounters with the test problems, we also show for each problem that the Levenberg-Marquardt algorithm fails to converge to a useful solution. For context, Moré and Wild (2009) also compared various derivative-free optimization algorithms (before the advent of the methods discussed here), but their work was not focused on inverting statistical observations and the comparison was done assuming a fixed computational budget (and consequently varying accuracy). The computational expense and importance of GCM calibration, however, more naturally leads to finding the most efficient algorithm for a fixed accuracy.

Our systematic experiments address several important aspects of ensemble-based optimization, relevant to GCM calibration.

1. We increase the complexity and dimensionality of the test problems, so our experiments can indicate which ensemble methods may have the greatest potential to scale to GCM calibration.
2. We investigate the role the prior plays in ensemble methods. Intuitively, a good, informative prior should accelerate the convergence and, hence decrease the computational cost of ensemble methods. Reliable priors, however, are not always available. Our experiments highlight which ensemble methods are robust to the lack of reliable prior knowledge.
3. One of our test problems features a neural network parameterization, this reflects an important recent direction in the context of GCM calibration where ML parameterizations are proposed to represent subgrid processes. The numerical ex-

- amples we present here are a first step towards understanding issues that may arise when using neural network parameterizations for GCM calibration.
4. We run many repeated test problems under random re-initializations, and provide quantitative statements regarding the robustness of our results and stability of the algorithms.

The rest of the paper is organized as follows. In Section 2 we briefly review the ensemble methods we compare. Section 3 describes the systematic numerical experiments: Definitions of forward models (including dynamics, parameterizations, and priors), statistical observations and associated error models, iteration stopping criteria, and optimal ensemble sizes. We report and discuss the outcome of the numerical experiments in Section 4 and conclude the paper with a summary of our findings in Section 5.

2 Variants of iterative ensemble methods

Iterative ensemble methods for parameter estimation originated from the ensemble Kalman filter (EnKF, Evensen (2009, 1994)), which has been vastly successful in numerical weather prediction (NWP), physical oceanography, and reservoir engineering. To stick to the example of NWP, the EnKF updates a forecast ensemble, generated by a numerical model, with atmospheric data. The mean of the updated ensemble represents the predicted state of the atmosphere and the ensemble itself represents variations in the atmospheric state that are compatible with the available data. The EnKF iterates this process, and each cycle of the EnKF assimilates the most recent observations.

Iterative ensemble methods use the EnKF formalism iteratively on *the same* data set. Since an EnKF update reduces variance, the spread of the ensemble shrinks in each iteration. In ensemble Kalman inversion (EKI), the repeated use of the same data causes the ensemble to ultimately collapse onto the minimizer of a loss function (see below). In iterative ensemble methods, e.g., IEKF or ESMDA, the collapse of the ensemble is prevented. As a result, the ensemble in iterative ensemble methods does not collapse and is approximately distributed according to a Bayesian posterior distribution (Emerick & Reynolds, 2013; Chen & Oliver, 2013; Carrillo et al., 2024).

2.1 The EKI loss function and notation

The loss function targeted by EKI is

$$\mathcal{L}(u) = \frac{1}{2} \left\| R_d^{-\frac{1}{2}} (d - \mathcal{F}(u)) \right\|^2 + \frac{1}{2} \left\| B^{-\frac{1}{2}} (m - u) \right\|^2, \quad (1)$$

where $\|\cdot\|$ denotes the two-norm, $\mathcal{F}(\cdot)$ is the nonlinear forward model mapping parameters u to the data d , and R_d is the data error covariance matrix. The first term in (1) describes how well the model fits the data, and the second term regularizes the optimizer to be close to the vector m , with ‘‘closeness’’ being specified by the symmetric positive definite matrix B . Within a Bayesian context, this loss forms the negative log-likelihood with the first term attributed to a Gaussian likelihood $p_l(d|u)$ and the second term attributed to a Gaussian prior $p_0(u)$ with mean m and covariance matrix B . The posterior distribution defined by the likelihood and prior, $p(u|d) = p_0(u)p_l(d|u)/p(d)$, is proportional to $p(u|d) \propto \exp(-\mathcal{L}(u))$.

The loss function (1) can be rewritten as

$$\mathcal{L}(u) = \frac{1}{2} \left\| R^{-\frac{1}{2}} (y - \mathcal{G}(u)) \right\|^2, \quad (2)$$

where

$$R = \begin{pmatrix} R_d & 0 \\ 0 & B \end{pmatrix}, \quad y = \begin{pmatrix} d \\ m \end{pmatrix}, \quad \mathcal{G}(u) = \begin{pmatrix} \mathcal{F}(u) \\ u \end{pmatrix}.$$

Here, $\mathcal{G}(\cdot)$ augments the model with the identity map, y is an extended observation (data and prior mean), and the extended observation error covariance is R (accounting for observation error covariances R_d and prior covariances B). The variants of EKI we describe below can all be compactly described with reference to the loss (2), but IEKF distinguishes the prior covariance B from the data error covariance R_d and, hence, is more conveniently described with reference to (1).

We use subscripts for the iteration and superscripts for the ensemble members, i.e., u_j^k is the k th ensemble member at iteration j . The various ensemble methods make use of normalized perturbation matrices

$$U_j = \frac{1}{\sqrt{n_e - 1}} (u_j^1 - \bar{u}_j \ u_j^2 - \bar{u}_j \ \cdots \ u_j^{n_e} - \bar{u}_j), \quad \bar{u}_j = \frac{1}{n_e} \sum_{k=1}^{n_e} u_j^k, \quad (3)$$

$$G_j = \frac{1}{\sqrt{n_e - 1}} (g_j^1 - \bar{g}_j \ g_j^2 - \bar{g}_j \ \cdots \ g_j^{n_e} - \bar{g}_j), \quad \bar{g}_j = \frac{1}{n_e} \sum_{k=1}^{n_e} g_j^k, \quad (4)$$

where $g_j^k = \mathcal{G}(u_j^k)$. Empirical covariance and cross-covariance matrices can be defined via the perturbation matrices as

$$C_j^{uu} = U_j U_j^\top, \quad C_j^{gg} = G_j G_j^\top, \quad C_j^{ug} = U_j G_j^\top, \quad (5)$$

which describe covariances between the unknowns (C_j^{uu}), between the predicted observation (C_j^{gg}), and cross-covariances between the unknowns and predicted observation (C_j^{ug}); here and below, superscript \top denotes the transpose.

2.2 Tikhonov regularized EKI

The iteration of a Tikhonov regularized EKI (TEKI, Chada et al. (2020)) is

$$u_{j+1}^k = u_j^k + \alpha \left\{ C_j^{ug} (C_j^{gg} + R)^{-1} (y - (g_j^k + \eta_j^k)) \right\}, \quad (6)$$

where η_j^k is a random sample from a Gaussian distribution with mean zero and covariance matrix R and where α is a step size (which we typically set to $\alpha = 1$). Note that (6) basically amounts to repeated EnKF updates using the same data y . The spread of the ensemble is reduced at each iteration, leading to TEKI ensemble collapse onto the minimizer of the loss (2) (Schillings & Stuart, 2017, 2018; Chada & Tong, 2019). Though iterations of TEKI and EKI are identical, the first paper on EKI (Iglesias et al., 2013) did not consider regularization or, equivalently, prior distributions.

2.3 Ensemble transform Kalman inversion

Ensemble transform Kalman inversion (ETKI, Huang, Huang, et al. (2022)) is based on the ensemble transform Kalman filter (ETKF, Bishop et al. (2001); Tippett et al. (2003)). During an iteration, ETKI updates the ensemble mean \bar{u}_j and the ensemble perturbations U_j separately. The update equation for the ensemble mean is

$$\bar{u}_{j+1} = \bar{u}_j + U_j (I + G_j^\top R^{-1} G_j)^{-1} G_j^\top R^{-1} (y - \bar{g}_j), \quad (7)$$

and the ensemble perturbations are updated by

$$U_{j+1} = U_j T, \quad T = (I + G_j^\top R^{-1} G_j)^{-\frac{1}{2}}, \quad (8)$$

where T is a *symmetric* $n_e \times n_e$ ensemble transform matrix. The ensemble for the next iteration is constructed by adding the updated perturbations (columns of the matrix U_{j+1}) to the updated ensemble mean \bar{u}_{j+1} :

$$u_{j+1}^k = \bar{u}_{j+1} + [U_{j+1}]_k \sqrt{n_e - 1}; \quad (9)$$

here $[U_{j+1}]_k$ is the k th column of U_{j+1} . To ensure that the ensemble mean is \bar{u}_{j+1} , one must chose a symmetric square root in (8). ETKI is numerically efficient for the common situation where the ensemble size n_e is smaller than the number of observations or the number of unknowns, because the method performs all computations in the *ensemble space*, so linear solves and matrix square roots are done with small matrices of size $n_e \times n_e$. ETKI is most efficient if one can efficiently compute the matrix $R^{-1}G_j$, such as common practical scenarios where R is low-rank, diagonal, or sparse. We note that the ETKI and TEKI updates are asymptotically equivalent, but for a finite ensemble size n_e the random perturbation in TEKI introduces an extra source of error compared to ETKI (Al-Ghattas & Sanz-Alonso, 2023).

2.4 Unscented Kalman inversion

Unscented Kalman inversion (UKI, Huang, Schneider, and Stuart (2022)) is based on the unscented Kalman filter (UKF, Wan and Van Der Merwe (2000)) and the unscented transform (Julier & Uhlmann, 1997). The basic idea is to use the unscented transform to define the ensemble by a quadrature stencil known as *sigma points*. There are various ways to define sigma points, but we follow Huang, Schneider, and Stuart (2022) and define the ensemble by the sigma points:

$$u_j^1 = \bar{u}_j, \quad (10)$$

$$u_j^{k+1} = \bar{u}_j + a\sqrt{n_u} [C_j^{uu}]_k \quad (1 \leq k \leq n_u), \quad (11)$$

$$u_j^{k+1+n_u} = \bar{u}_j - a\sqrt{n_u} [C_j^{uu}]_k \quad (1 \leq k \leq n_u). \quad (12)$$

Here, a is a hyper-parameter that we set to one and $[C_j^{uu}]_k$ is the k th column of the Cholesky factor of C_j^{uu} ; for the first iteration, $C_0^{uu} = B$ and $\bar{u}_0 = m$. The ensemble mean and covariance matrix are updated using

$$\bar{u}_{j+1} = \bar{u}_j + C_j^{ug} (C_j^{gg} + a^2 R)^{-1} (y - \bar{g}_j), \quad (13)$$

$$C_{j+1}^{uu} = C_j^{uu} - C_j^{ug} (C_j^{gg} + a^2 R)^{-1} \left(\frac{1}{a^2} C_j^{ug} \right)^\top, \quad (14)$$

and the UKI ensemble u_{j+1}^k is generated by computing new sigma points from \bar{u}_{j+1} and C_{j+1}^{uu} . Importantly, the ensemble size of UKI is fixed:

$$n_e = 2n_u + 1. \quad (15)$$

This can be efficient when the dimension n_u of the parameter space is small, but becomes problematic when n_u is large (as expected in GCM calibration), because each ensemble member requires a forward model evaluation, which can be computationally expensive.

2.5 The iterative ensemble Kalman filter

The iterative ensemble Kalman filter (IEKF) was first proposed by Chen and Oliver (2013) and later studied by Chada et al. (2021) (who refer to it as IEKF with statistical linearization). IEKF is derived from the Gauss-Newton update and uses an ensemble approximation for the Jacobian of the forward model $\mathcal{F}(\cdot)$, including the normalized perturbation matrix

$$F_j = \frac{1}{\sqrt{n_e - 1}} (f_j^1 - \bar{f}_j \ f_j^2 - \bar{f}_j \ \cdots \ f_j^{n_e} - \bar{f}_j), \quad \bar{f}_j = \frac{1}{n_e} \sum_{k=1}^{n_e} f_j^k, \quad (16)$$

where $f_j^k = \mathcal{F}(u_j^k)$. Specifically, at iteration j , the Jacobian approximation is

$$J_j = F_j U_j^\dagger, \quad (17)$$

where the superscript \dagger denotes a pseudo-inverse. With this Jacobian approximation, IEKF iteration is

$$u_{j+1}^k = u_j^k + \alpha \{ K_j (d - (f_j^k + \varepsilon_j^k)) + (I - K_j J_j) (m - (u_j^k + \zeta_j^k)) \}, \quad (18)$$

where

$$K_j = B J_j^\top (J_j B J_j^\top + R_d)^{-1}, \quad (19)$$

$$\varepsilon_j^k \sim \mathcal{N}(0, 2\alpha^{-1} R_d), \quad (20)$$

$$\zeta_j^k \sim \mathcal{N}(0, 2\alpha^{-1} B). \quad (21)$$

We note that there are slight differences between IEKF of Chen and Oliver (2013) and Chada et al. (2021) regarding the scaling of the random perturbations ε_j^k and ζ_j^k . In the numerical experiments below, we use the implementation described by Chada et al. (2021), but similar results are obtained when we use the implementation originally proposed by Chen and Oliver (2013).

2.6 Derivative-based optimization with Levenberg-Marquardt

The Levenberg-Marquardt (LM, Levenberg (1944); Marquardt (1963); Nocedal and Wright (2006)) method is a derivative-based algorithm for solving nonlinear least squares problems. To derive the LM update equations, we write the loss function (2) as the two-norm of a residual $r(u)$,

$$\mathcal{L}(u) = \frac{1}{2} \|r(u)\|^2, \quad r(u) = R^{-\frac{1}{2}}(y - \mathcal{G}(u)). \quad (22)$$

In LM, the residual $r(u)$ is approximated by its linearization around the current iterate u_j and an increment $\Delta u_j = u_{j+1} - u_j$ is defined by the solution of the regularized linear least squares problem

$$\min_{\Delta u_j} \frac{1}{2} \left\| r(u_j) + \frac{\partial r}{\partial u}|_{u_j} \Delta u_j \right\|^2 + \frac{1}{2\lambda} \|\Delta u_j\|^2, \quad (23)$$

where $\lambda > 0$ is a damping factor adjusted during the iterations and where $\frac{\partial r}{\partial u}|_{u_j}$ is the Jacobian of the residual, evaluated at the current iteration u_j . Writing the Jacobian of $r(u)$ in terms of the Jacobian of the generalized model \mathcal{G}

$$\frac{\partial r}{\partial u} = -R^{-\frac{1}{2}} \frac{\partial \mathcal{G}}{\partial u}, \quad (24)$$

and substitution into (23) gives

$$\min_{\Delta u_j} \frac{1}{2} \left\| R^{-\frac{1}{2}} ((y - \mathcal{G}(u_j)) - D_j \Delta u_j) \right\|^2 + \frac{1}{2\lambda} \|\Delta u_j\|^2, \quad (25)$$

where we introduced the shorthand notation $D_j = \partial \mathcal{G} / \partial u|_{u_j}$ for the Jacobian of the generalized model, evaluated at the current iterate u_j . The solution of this least squares problem is

$$\Delta u_j^* = \lambda D_j^\top (\lambda D D_j^\top + R)^{-1} (y - \mathcal{G}(u_j)), \quad (26)$$

so that the LM update equation becomes

$$u_{j+1} = u_j + \Delta u_j^* = u_j + \lambda D_j^\top (\lambda D D_j^\top + R)^{-1} (y - \mathcal{G}(u_j)). \quad (27)$$

We use LM within Python and SciPy's `least_squares` algorithm, which in turn is a wrapper around the MINPACK Fortran library. In our numerical experiments, LM is a representative of derivative-based optimization methods and we compare LM to ensemble-based methods in all numerical experiments.

3 Experiment design

Our numerical experiments are designed to explore the applicability of ensemble methods for GCM calibration. The basic idea is to define a forward model using a chaotic dynamical system that depends on model parameters or parameterizations. We apply various ensemble methods (TEKI, ETKI, UKI, IEKF) to estimate model parameters or parameterizations from time-averaged data. We then measure the computational cost each ensemble method requires to find a solution with a specified accuracy.

We define the dynamics, model parameters, and parameterizations in Section 3.1, with prior distributions over model parameters/parameterizations described in Section 3.2; we compute the observation error covariance matrix R_d via the strategy outlined by Cleary et al. (2021). The only tunable parameter of the ensemble methods is the ensemble size n_e ; we compute and use an optimal ensemble size that maximizes computational efficiency (Section 3.3). Section 3.4 defines the exit criteria for optimization iterations that ensures that each ensemble method finds parameters or parameterizations that lead to similar model-data misfits, or target accuracies. In our experiments, we assess the computational cost of EKI variants by the number of forward model runs needed to reach the target accuracy. This is a reasonable proxy for the computational cost of an ensemble method, because GCM simulations are computationally more expensive than the linear algebra required for EKI ensemble updates.

Systematic numerical experiments like this are currently out of reach with GCMs: Our strategies for computing the observation error covariance matrix or the optimal ensemble size are too expensive for GCMs. To reduce the computational burden of the numerical experiments, we use systems of chaotic ordinary differential equations (Lorenz-type problems, see Section 3.1) instead of GCMs. While this is a drastic simplification, the numerical experiments with simplified dynamics can systematically investigate some important aspects of ensemble-based methods, relevant to GCM calibration. We also repeat such experiments under different initialization to get robust conclusions. We thus investigate which ensemble methods have the greatest *potential* to scale to GCM calibration along with the importance of informative versus uninformative prior information. One of our test problems includes a neural network parameterization and the implied loss function is not only noisy, but also non-convex. Our test problems highlight how changes to the loss landscape can impact the ensemble methods' ability to minimize the loss function.

3.1 Forward models, time-averaged data and error models

The forward model $\mathcal{F}(\cdot)$ is the process of simulating a dynamical model for τ time units and subsequently computing statistics of the simulation output. The forward model for time-averaged data is illustrated by a flowchart in Figure 1, and explained in detail below.

3.1.1 Dynamics and parameterizations

In our experiments, the dynamical models are Lorenz-type, chaotic, ordinary differential equations (ODE) which we discretize with a fourth-order Runge-Kutta scheme. Specifically, we will use the Lorenz '63 model (L'63, Lorenz (1963))

$$\frac{dz_1}{dt} = \sigma(z_2 - z_1), \quad \frac{dz_2}{dt} = \rho z_1 - z_2 - z_1 z_3, \quad \frac{dz_3}{dt} = z_1 z_2 - \beta z_3, \quad (28)$$

where σ , ρ and β are model parameters. In the numerical experiments in Section 4.1, we estimate ρ and β , but fix $\sigma = 10$. We also consider the Lorenz '96 model (L'96, Lorenz (1995)), defined by the ODE

$$\frac{dz_l}{dt} = z_{l-1}(z_{l+1} - z_{l-2}) - z_l + \phi_l, \quad l = 1, \dots, n_z, \quad (29)$$

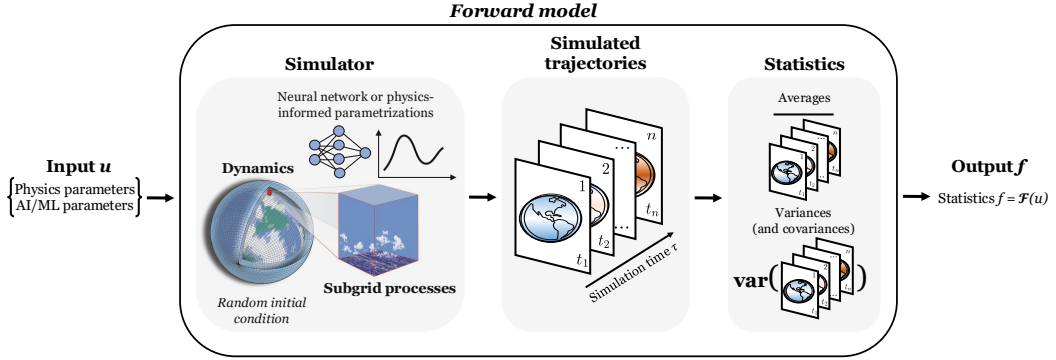


Figure 1. Flow chart of a forward model $\mathcal{F}(\cdot)$ whose outputs are statistics of the system state. For a given set of parameters u , the forward model first simulates the dynamics for a time period τ , starting from a random initial condition. The statistics $f = \mathcal{F}(u)$ are subsequently computed from the simulation output after a spin-up period. (Image of dynamics and subgrid processes simulation is from Schneider, Teixeira, et al. (2017).)

on a periodic domain, where ϕ_l is a forcing. We use the L'96 model with two different forcings:

1. The classical constant forcing

$$\phi_l = \phi = 8, \quad l = 1, \dots, n_z. \quad (30)$$

2. A spatially varying forcing (Vishny et al., 2024),

$$\phi_l = 8 + 6 \sin\left(\frac{4\pi}{n_z}l\right), \quad l = 1, \dots, n_z. \quad (31)$$

In the case of a constant forcing, the ensemble methods estimate ϕ (Section 4.2). To emulate the effects of parameterizations in GCMs, we consider different parameterizations of the spatially varying forcing: A grid-based parameterization, i.e., we define each ϕ_l separately (as is the case in the actual dynamics), and a neural network parameterization. The latter setup mimics, to some extent, climate models with subgrid processes parameterized by neural networks. Note that in the grid-based configuration, the ensemble methods estimate ϕ_l on the grid (Section 4.3), but in the neural network parameterization, the ensemble methods estimate the weights and biases of a neural network that parameterizes the forcing (Section 4.4). The different parameterizations of the forcing result in different numbers of unknowns across the test problems; we further vary the dimension n_z to design test problems with different complexities. The various configurations of the dynamics and parameterizations are summarized in Table 1.

3.1.2 Time-averaged data and associated error models

We consider estimation of model parameters or parameterizations from time-averaged data. The forward model thus amounts to simulating the dynamics for a time interval τ , starting from a randomized initial condition $z(0)$, followed by evaluating first- and second-order moments of the system state after a “spin-up period” (Dunbar et al., 2021; Cleary et al., 2021). The randomized initial condition implies a spin-up, during which the influence of a randomly chosen initial condition is “forgotten” by the chaotic dynamics.

Dynamics	Parameterization (u)	# of unknowns (n_u)	State dimension (n_z)
L'63	Model parameters ρ, β	2	3
L'96	Model parameter ϕ	1	40
L'96	Grid-based ϕ_l	40	40
L'96	Neural net parameterized ϕ_l	61	100

Table 1. Summary of the dynamical models and parameterizations in our numerical experiments. The dynamics are Lorenz models (L'63 or L'96). The parameterizations determine n_u parameters – either model parameters or parameterizations. The number of unknowns is, in general, different from the number of state variables of the dynamics or the number of statistical observations.

For the L'63 dynamics, the statistics are the mean, variances, and covariances of the three state variables (Cleary et al., 2021):

$$\mathcal{F}_{\text{L}'63}(u) = (\bar{z}_1, \bar{z}_2, \bar{z}_3, \text{var}(z_1), \text{var}(z_2), \text{var}(z_3), \text{cov}(z_1, z_2), \text{cov}(z_1, z_3), \text{cov}(z_2, z_3)). \quad (32)$$

For the L'96 dynamics, the statistics are the mean and standard deviations of the n_z state variables:

$$\mathcal{F}_{\text{L}'96}(u) = (\bar{z}_1, \dots, \bar{z}_{n_z}, \sqrt{\text{var}(z_1)}, \dots, \sqrt{\text{var}(z_{n_z})}). \quad (33)$$

An important characteristic of the forward model is that it is noisy, i.e., a fixed parameter u may result in different model outputs f . The noise is caused by the randomized (unknown) initial condition and the short simulation time τ . Specifically, let $\mathcal{F}_\infty(\cdot)$ denote the statistics one would compute from an *infinitely long* simulation (for any initial condition). Then

$$\mathcal{F}(u, z(0)) \approx \mathcal{F}_\infty(u) + \frac{1}{\sqrt{\tau}} \xi, \quad (34)$$

where ξ is normally distributed with mean zero (Cleary et al., 2021). In other words, the noise level is related to the duration of the simulation τ . The longer the time window, the less noisy are the statistics we compute; a shorter time window leads to noisier statistics.

We make use of (34) to define the observation error covariance R_d (Cleary et al., 2021). Recall that the data are statistical quantities computed from a simulation of duration τ . To compute the observation error covariance, we run a simulation of duration $n_s \cdot \tau$ and then window the simulation output to compute n_s samples of statistical data associated with a simulation duration τ . The observation error covariance is then simply the sample covariance. This strategy of computing R_d naturally takes into account that the noise in the statistical data decreases with the simulation time τ , but requires a rather long overall simulation time ($n_s \cdot \tau$), rendering this strategy perhaps infeasible for GCM calibration (though sampling-error estimators can help (Vishny et al., 2024; Ledoit & Wolf, 2022)). Moreover, more statistical data requires a longer simulation for accurate, sample-based estimates of the observation error covariance matrix.

Table 2 summarizes the simulation time τ , the spin-up, and the number of simulations we use for the construction of the observation error covariance matrix R_d in the numerical experiments. Note that the simulation times are relatively short, which renders the forward models and implied loss functions noisy (too noisy for derivative-based optimization, as we will demonstrate). The number of simulations used to estimate the observation error covariance matrix (n_s) scales with the number of data n_d , to ensure accuracy in each setting. Since we are computing statistics for each state variable, the number of data n_d scales with the number of states n_z . For GCMs, such long simulation times may be overly expensive, but with our simplified setup, accurate modeling

Dynamics	Parameterization (u)	Sim. time (τ)	# of sims. (n_s)	Spin-up	# of data
L'63	Model param. ρ, β	10	36	30	9
L'96	Model param. ϕ	10	800	4	80
L'96	Grid-based ϕ_i	50	800	4	80
L'96	Neural Net	50	2000	4	200

Table 2. Summary of the specifications the forward models use in the numerical experiments.

The dynamics are Lorenz models (L'63 or L'96). The inversions recover different parameters, defined by different types of parameterizations. The inversions compute statistical quantities based on a simulation of the dynamics of duration τ . The construction of the observation error covariance matrix R_d is based in a simulation of duration $n_s \cdot \tau$. Statistical data are computed after a spin-up period during which the influence of unknown initial conditions is forgotten.

of errors due to chaotic internal variability is feasible. In particular, measurement errors also arise, but play no role in our perfect model experiments.

3.1.3 Summary of the forward model: dynamics, parameterizations, statistical data and observation errors

In summary, we have defined the forward models $\mathcal{F}(\cdot)$ that use different dynamics and model parameters or parameterizations. The forward model maps model parameters/parameterizations to statistical data, and we described how to accurately model errors in these data arising from chaotic internal variability via a careful construction of the observation error covariance matrix R_d . For a controlled, systematic numerical experiment, we can generate synthetic data as follows: We apply the forward model $\mathcal{F}(\cdot)$ to a “true” parameter set u_{true} and “true” initial condition $z_{\text{true}}(0)$ to obtain the statistical quantities $d = \mathcal{F}(u_{\text{true}}, z_{\text{true}}(0))$; the data.

We emphasize again that the statistical data are generated with an initial condition that is unknown to the ensemble methods we use to recover the true parameter set (the initial condition is randomized in the forward model). The fact that the initial conditions need not be computed is an advantage of using statistical data.

3.2 Prior distributions

For the L'63 dynamics, we follow Cleary et al. (2021), and define the prior as independent log-normal distributions with location and scale parameters corresponding to $m = (3.3, 1.2)$ and $B = \text{Diagonal}(0.5^2, 0.15^2)$ (i.e., we take a Gaussian prior and exponentiation in the forward map); this prior distribution yields positive distributions for ρ and β with means (30.7, 3.36), and with a (0.05, 0.95) quantile range of (11.9, 61.6) for ρ and (2.59, 4.25) for β . The true parameter values are $\rho = 28$ and $\beta = 8/3$, lying in a region of high prior probability.

For the L'96 dynamics with constant forcing, the prior is centered close to the true forcing with prior mean $m = 10$ and standard deviation 4. As before, the true parameter value is in the region of high prior probability. For L'96 with spatially variable forcing and a grid-based parameterization, the prior mean is $m = (8, \dots, 8)$ and the elements B_{ij} of the prior covariance are

$$B_{ij} = 9 \exp\left(-\frac{1}{2}|i - j|\right). \quad (35)$$

Again, the true parameter values are well within the region of high prior probability.

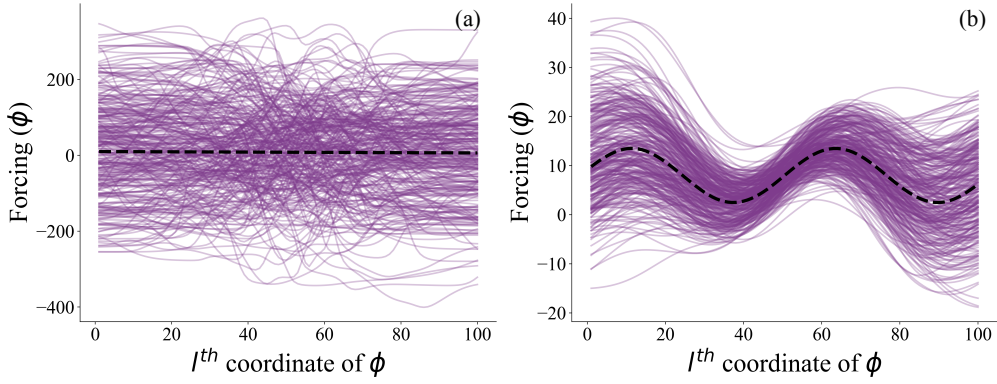


Figure 2. Random samples taken from the prior distributions constructed for the L'96 model with a neural network parameterization. The purple lines are the functions generated by neural networks whose weights and biases are draws from a Gaussian prior. The black dashed lines are the prior means. (a) Samples from the “uninformative” prior. (b) Samples from the “informative” prior.

The construction of the prior for the L'96 model with a neural network parameterization is more difficult, because there are no clear guidelines for how to construct informative prior distributions for weights and biases of a neural network. To this end, we do not present a thorough investigation of different network prior ansatz or implementations. Instead we contrast two such contexts that lead to two very differently structured prior distributions to evaluate the effect on calibration performance.

First, we look at an empirically constructed Gaussian ensemble over network parameter sets, with each parameter-set arising from fitting a NN to a smooth function (Vishny et al., 2024). We generate random smooth functions by drawing samples from a smooth, periodic Gaussian process with a Gaussian kernel and length scale $\ell = 8$ and train neural networks on each draw. The results are sets of weights and biases that correspond to smooth functions. We then use these weights and biases to define the prior mean m and prior covariance B . We note that draws from this prior result in weights and biases for neural networks whose outputs do not necessarily resemble draws from the Gaussian process the networks were trained on. The prior is therefore rather poor and we inflate it by a factor of four in our numerical experiments for numerical stability of the EKI variants. We label this prior as the uninformative prior. Figure 2(a) illustrates the outputs (forcings) of neural networks whose weights and biases were drawn from the prior. The large spread in the functions illustrates that this prior is uninformative, both about the weights of the neural networks and about the corresponding forcing functions.

As a second contrastive approach, we define a Gaussian directly as a local perturbation of weights from one NN fit to a function that is closer to the true function. Precisely, we define the mean m as the weights and biases learned from training a neural network offline on a randomly translated and compressed version of the true forcing function and chose a diagonal covariance matrix $B = 0.1I_{n_u}$. Figure 2(b) shows the outputs of neural networks with weights and biases drawn from this prior. We note that the resulting functions closely resemble the true forcing and, hence this prior is more informative than the prior based simply on the assumption that the forcing be smooth. We label this prior as the informative prior. We will use both the informative and uninformative priors in our numerical examples to illustrate how priors affect the robustness and numerical efficiencies of ensemble methods. Note that the offline-online approach used here for the informative prior is also discussed by Pahlavan et al. (2024) and that sim-

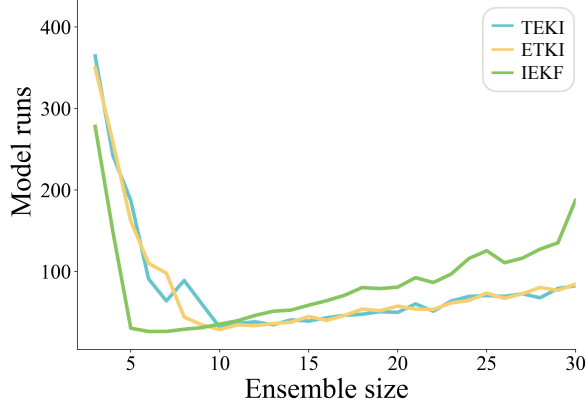


Figure 3. Average number of forward model runs required to reach a target RMSE of one as a function of ensemble size for the L'63 test problem. Shown are results for TEKI (blue), ETKI (yellow) and IEKF (green). For UKI, the ensemble size is fixed (Section 2.4)

ilar work on constructing reliable priors for neural networks includes Kozyrskiy et al. (2023); Arbel et al. (2023).

3.3 Optimal ensemble size of EKI

All ensemble methods, except UKI, require that the ensemble size n_e be specified. This raises the question of how to chose the ensemble size. A large ensemble size ensures accurate gradient approximations, and the EKI variants can reach the target accuracy with fewer iterations. If the ensemble size is small, the gradient approximations are inaccurate and more iterations are required, but each iteration is computationally less costly. An optimal ensemble size resolves the trade off between fewer iterations with a large ensemble size and more iterations with a smaller ensemble size. The optimal ensemble size results in the lowest computational cost required to reach a desired target accuracy, where we measure computational cost by the number of forward model runs performed.

To determine the optimal ensemble size we solve the same problem for a range of ensemble sizes and we keep track of how many forward model runs were performed. The number of iterations depends on the initial ensemble and the initial conditions for the simulations, which we chose at random, by drawing the initial ensemble from the prior and by perturbing the initial condition. Thus, the computational cost required is also random. We address this issue by performing 100 experiments (at each ensemble size) and then present the average of the number of forward model runs as an indicator of the computational cost.

An example of the average number of forward model runs required to reach a target accuracy as a function of the ensemble size is shown in Figure 3. We present results for the test problem with L'63 dynamics, but the results are qualitatively similar for the other test problems.

While the curves are somewhat noisy, we can clearly see that there is an optimally small ensemble size – larger ensemble sizes lead to the same result, but at a larger computational cost. The elevated computational cost for smaller ensemble sizes (smaller than optimal) are partially caused by ensemble failure, i.e., the ensemble was unable to reach the target accuracy within a maximum number of iterations (between 100-200 depending on the test problem). For this example, we note that the results for ETKI and TEKI are quite similar (which we observe in other examples as well), and that IEKF has a rather

small optimal ensemble size ($n_{e,\text{opt}} = 6$ for IEKF, compared to $n_{e,\text{opt}} = 10$ for TEKI and ETKI). Finally, we note that the graphs can asymptote at different slopes (consider all three graphs in Figure 3 for relatively large n_e). The reason is that IEKF requires more iterations than TEKI or ETKI, even if the ensemble size is large. This underlines our definition of optimal ensemble size: IEKF requires more iterations (for any ensemble size), but can reach the target accuracy with a small ensemble size; TEKI and ETKI require fewer iterations once the ensemble size is large enough (i.e., larger than the optimal ensemble size), but the resulting number of ensemble members is larger than for IEKF.

3.4 EKI stopping criteria

Derivative-based optimization algorithms typically stop the iteration once convergence is detected, e.g., because the loss function does not change much from one iteration to the next. We use a different strategy that emphasizes accuracy: Rather than checking for convergence of the ensemble (or its mean), we check if a desired accuracy is reached (independently of convergence). If a desired accuracy is reached, we stop the iteration. We chose this accuracy-based exit criteria for two reasons.

1. Accuracy is perhaps most important for GCM calibration. Once the model fits the data adequately, we may no longer want to invest computational resources to ensure that the iteration has converged.
2. The various ensemble methods may converge to solutions with different accuracies, which makes a systematic comparison difficult, because one needs to assess, in hindsight, how the relative computational costs compare to the achieved accuracies.

Accuracy-based exit criteria will ensure that each method attempts to achieve the same target accuracy, and we can systematically measure the computational expense required to achieve it. If an ensemble method is unable to achieve the target accuracy, the associated computational cost is large because the iteration continues until a large number of maximum iterations n_{\max} is reached.

We assess the accuracy by the root mean square error (RMSE) defined as

$$\text{RMSE}_j = \frac{1}{\sqrt{n_d}} \left\| R_d^{-\frac{1}{2}} (d - \mathcal{F}(\bar{u}_j)) \right\|, \quad (36)$$

where \bar{u}_j is the ensemble mean at iteration j . The EKI iterations stop once the RMSE is below a target RMSE. A good target is $\text{RMSE} = 1$, because then the errors in the simulated data are comparable to the errors we expect, as defined by the observation error covariance R_d . In our numerical experiments, we use an $\text{RMSE} = 1$ as our default choice, but also consider slightly larger target values of $\text{RMSE} = 1.1$ or $\text{RMSE} = 1.2$ to see if we can achieve computational speed up by sacrificing some accuracy.

3.5 Summary of the experimental setup

We perform the same systematic numerical experiments for the dynamics/parameterizations and resulting forward models described in Section 3.1. The experimental setup consists of the following steps.

1. Estimate the observation error covariance matrix R_d (Section 3.1.2).
2. Compute the optimal ensemble size for each ensemble method (Section 3.3).
3. For each ensemble method, determine how many forward model runs are needed to reach the target RMSE (at optimal ensemble size), using the stopping criteria described in Section 3.4.

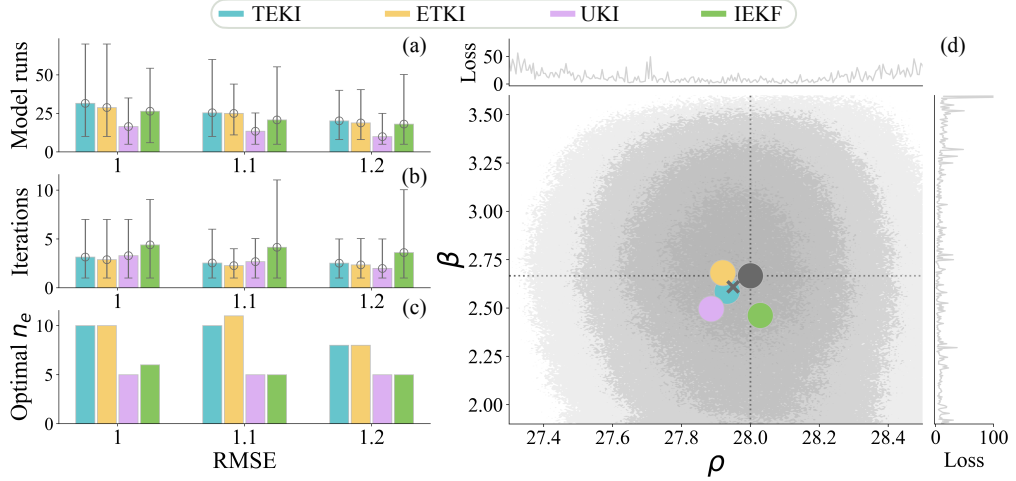


Figure 4. Summary of results for estimating two model parameters from statistics of L'63 dynamics. (a) Average number of forward model runs required to reach target accuracies of RMSE = 1, RMSE = 1.1, or RMSE = 1.2. (b) Average number of iterations required to reach the target accuracies. The error bars in panels (a) and (b) are derived from the 5th and 95th percentiles. (c) Optimal ensemble sizes for three target accuracies. (d) Parameter combinations in the ρ – β plane. The light gray contours are a 2D histogram of an averaged posterior distribution (darker grays represent regions of higher posterior probability and lighter grays represent regions of lower posterior probability). The ensemble means of TEKI, ETKI, UKI and IEKF are shown as blue, yellow, pink, and green dots. The true parameter pair is a dark gray dot and the expected posterior mode is a dark gray cross. Slices of the loss function obtained by varying ρ or β independently and separately are shown at the top and right sides of panel (d).

The various ensemble methods are all initialized with ensemble members drawn from the prior (Section 3.2). We repeat these experiments for different target accuracies to check if we can reduce the computational cost by sacrificing some accuracy.

4 Numerical experiments

We report the results of the numerical experiments and focus on the ensemble methods. Specifically, we discuss the computational cost, as measured by the number of forward model runs, the number of iterations required and the optimal ensemble size. Variations in these quantities are due to the randomization of the initial ensemble (which affects TEKI, ETKI and IEKF) and the random initial condition (which affects all four methods, TEKI, ETKI, IEKF and UKI). The optimal ensemble size is obtained by averaging over 100 experiments with random initial conditions and initial ensemble draws and, hence, is not random in our setup for TEKI, ETKI and IEKF. The ensemble size of UKI is always set by the number of unknown parameters (see equation (15)). For all experiments, we consider three different accuracies, corresponding to target RMSEs of 1, 1.1 and 1.2 (higher target RMSE implying lower accuracy). Optimization results with a derivative-based Levenberg-Marquardt (LM) algorithm are briefly summarized in Section 4.5.

4.1 Lorenz'63 dynamics

We illustrate the results with L'63 dynamics in Figure 4. Panels (a)-(c) show the

number of model runs required to reach the target RMSE, the number of iterations required and the optimal ensemble size – and we note that the number of model runs is simply the product of the number of iterations and the optimal ensemble size. For all three target RMSEs, the UKI requires the smallest average number of model runs. The uncertainty (5th and 95th percentiles) in the number of required model runs is induced by the randomization over initial conditions, which in turn leads to a varying number of iterations (between two and four). The ensemble size of UKI is fixed at $n_e = 5$, so that the overall cost, which equals the number of iterations multiplied by the ensemble size, amounts to 10-20 forward model runs, depending on the target RMSE and the initial conditions. We note that the ensemble size of UKI is small ($n_e = 2 \cdot 2 + 1 = 5$) because we only estimate two model parameters (ρ and β , see (15)).

The average cost of IEKF is larger than for UKI, but less than the average cost of TEKI or ETKI. The low average cost is due to the small optimal ensemble size of IEKF (between $n_e = 5$ and $n_e = 6$). IEKF however, is not very robust because the variation in the number of iterations is large, ranging from two to ten for all target RMSEs. Large variations in the number of iterations then translate into a large variation in the number of model runs.

TEKI and ETKI are comparable in terms of their computational cost, optimal ensemble size and required number of iterations. The uncertainties in the number of iterations is also comparable for TEKI and ETKI and it decreases as the target RMSE increases. We also note that TEKI and ETKI require fewer iterations, but a larger optimal ensemble size than IEKF. The number of required iterations and the optimal ensemble size, however, can trade off to lead to similar computational costs of these algorithms (on average).

In this problem, UKI is the algorithm of choice because it requires the smallest number of forward model runs for all target RMSEs, even when taking into account uncertainties due to the randomized initial ensembles and initial conditions. The average cost of IEKF is smaller than the average cost of TEKI or ETKI, but the variation (or uncertainty) in the computational cost of IEKF is larger than the variation of the cost of TEKI or ETKI. Moreover, the variation in the computational cost of TEKI or ETKI decreases as we increase the target RMSE (lower the specified accuracy). The large uncertainties associated with the average cost of IEKF make this algorithm less attractive to use than TEKI or ETKI.

We illustrate the parameter estimates of TEKI, ETKI, UKI and IEKF and the loss landscape of this parameter estimation problem in Figure 4(d). Specifically, we show the ensemble means of TEKI, ETKI, UKI and IEKF after the final iteration in the $\rho - \beta$ plane for one of our experiments. Since we require that each ensemble method reaches the same target RMSE, the methods find similar model parameters, which are close to the true model parameters. The gray contours in Figure 4(d) correspond to the expected negative logarithm of the posterior distribution, which we compute by evaluating the loss function (equation (1)) over a grid and averaging. The true parameter value, as well as the estimates of TEKI, ETKI, UKI or IEKF are all clustered in the region where the averaged loss function is small or, equivalently, where the averaged posterior probability is high. The top and side panels of Figure 4(d) show slices through the loss function, holding one of two parameters fixed at the true value. These slices highlight that the loss function is noisy and characterized by many local minima. For these reasons, derivative-based optimization converges to the local minimum closest to the starting point of the iteration. The local minimum identified by derivative-based optimization is often characterized by a large data misfit (see also Section 4.5).

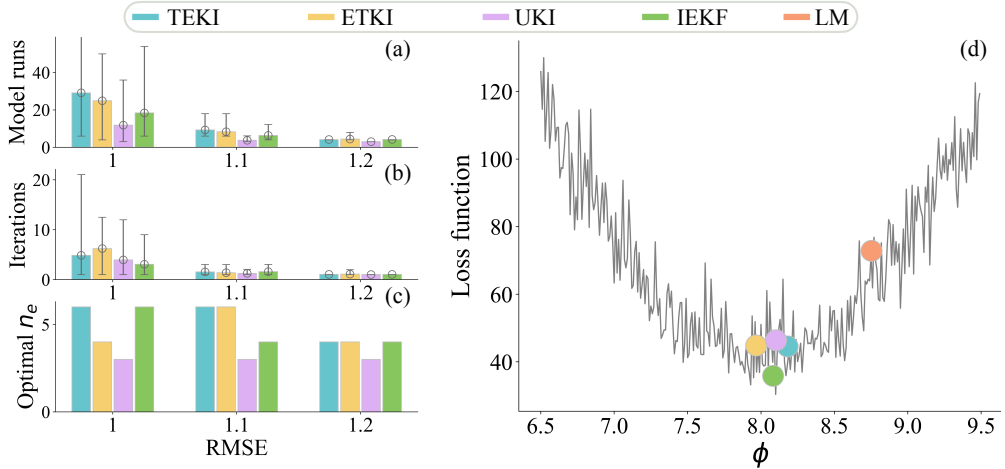


Figure 5. Summary of results for the model parameter estimation problem with L'96 dynamics under a constant forcing. (a) Average number of forward model runs required to reach target accuracies of RMSE = 1, RMSE = 1.1, or RMSE = 1.2. (b) Average number of iterations required to reach the target accuracies. The error bars in panels (a) and (b) are derived from the 5th and 95th percentiles. Note the truncated *y*-axis in panel (a). (c) Optimal ensemble sizes for three target RMSEs. (d) Loss function and ensemble means of TEKI, ETKI, UKI and IEKF for one of our experiments. Also shown is the result of a derivative-based optimization via LM, which fails to converge to a useful solution (defined as RMSE ≤ 1.2).

4.2 Lorenz'96 dynamics: constant forcing

Results obtained with L'96 dynamics under a constant forcing are summarized in Figure 5. All methods relatively struggle to reach a target RMSE of one compared to larger RMSEs, which can be deduced from the large variation in the number of iterations required. In particular, TEKI often requires up to 20 iterations to reach the target RMSE of one. All ensemble methods can more reliably reach the target RMSEs 1.1 and 1.2, and the variation in the number of iterations or forward model runs decreases with increasing target RMSE.

Because we only estimate one unknown, the ensemble size of UKI is $n_e = 3$, which is smaller than the optimal ensemble sizes we determine for TEKI, ETKI or IEKF (ranging from $n_e = 4$ for IEKF and $n_e = 4, \dots, 6$ for TEKI and ETKI). The number of iterations required are comparable for all four algorithms and, hence, the UKI incurs the lowest computational cost (for all target RMSEs). For a target RMSE of 1.1, IEKF is more efficient than TEKI or ETKI, taking into account uncertainties due to the initial ensemble draw/the initial conditions. For a target RMSE of 1.2, the efficiency of all four methods is practically independent of the initial ensemble or the initial condition – we do not observe significant variation in the number of iterations required. At a lower accuracy (RMSE of 1.2), the computational costs of all four methods are comparable, but UKI incurs the smallest cost due to the small ensemble size (and small number of unknowns).

In summary, we find that all four methods have relatively large variability when the target RMSE is one (desired accuracy is high) and that all methods are more robust and comparable in terms of their computational costs when the target RMSE is larger (RMSE=1.2, i.e., the accuracy is lower). At an intermediate accuracy (target RMSE of 1.1), UKI is most efficient and IEKF is more efficient and more reliable than TEKI or

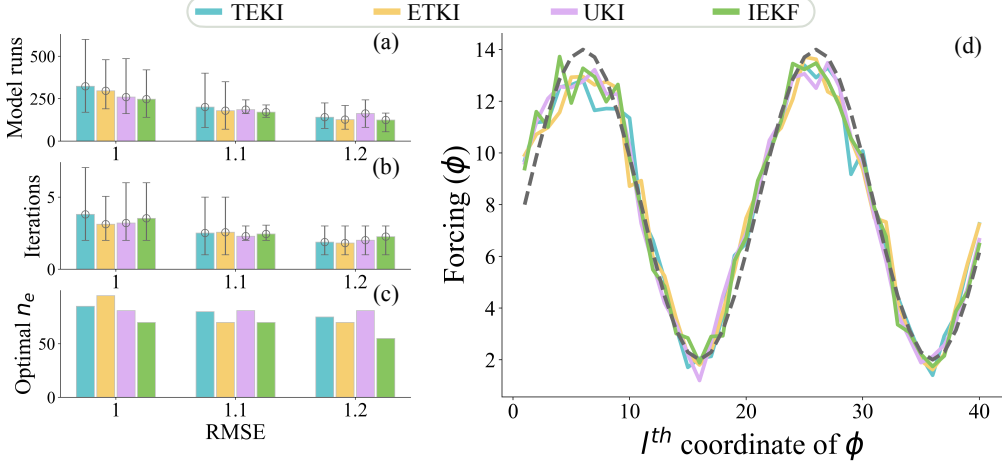


Figure 6. Summary of results for L'96 dynamics under a spatially varying forcing, parameterized on a grid. (a) Average number of forward model runs required to reach target accuracies of $\text{RMSE} = 1$, $\text{RMSE} = 1.1$, or $\text{RMSE} = 1.2$. (b) Average number of iterations required to reach the target accuracies. The error bars in panels (a) and (b) are derived from the 5th and 95th percentiles. (c) Optimal ensemble sizes for three target RMSEs. (d) Spatially varying forcing ϕ_l (black, dashed) and estimated grid-based parameterizations obtained by TEKI (blue), ETKI (yellow), UKI (pink), and IEKF (green).

ETKI. Again, we note that the computational efficiency of UKI is tied to the fact that the number of unknowns is so small (we only estimate one parameter).

Figure 5(d) illustrates the loss landscape (not averaged, target RMSE of one). The ensemble methods (TEKI, ETKI, UKI and IEKF) can leverage the large scale convexity of the loss function, even though locally the loss function is not convex at all (many local minima). Derivative-based techniques, e.g., Levenberg-Marquardt, cannot utilize the large scale convexity but rather converge to the local minimum closest to their initialization (see Section 4.5).

4.3 Lorenz'96 dynamics: spatially varying forcing and a grid-based parameterization

We now consider L'96 dynamics under a spatially varying forcing, with the forcing function parameterized on the grid, i.e., in the same way the forcing acts on the model that is used to generate the synthetic data. For this grid-based forcing, the number of unknowns is $n_u = 40$, so that the ensemble size for UKI is $n_e = 2 \cdot 40 + 1 = 81$. The optimal ensemble sizes of TEKI and ETKI are slightly larger for a target RMSE of 1, but comparable or smaller for target RMSE of 1.1 or 1.2. The optimal ensemble size of IEKF is smaller than the ensemble size of UKI or TEKI and ETKI for all three target RMSEs.

The number of iterations required and the associated uncertainties are comparable for IEKF and UKI, which means that IEKF, in this example, is computationally more efficient than UKI. For a target RMSE of one, ETKI has the smallest uncertainty in the number of iterations among all methods, but it also has the largest ensemble size, so that the computational cost is, on average, larger than the cost of UKI or IEKF. TEKI has the largest uncertainty in the number of iterations and overall also the largest computational cost when the target RMSE is set to one. TEKI and ETKI are comparable at

a target RMSE of 1.1, but UKI or IEKF are more efficient. For a larger target RMSE, TEKI, ETKI and IEKF are comparable in their computational cost and associated uncertainties and all three are more efficient than UKI.

In summary, IEKF is the most reliable and efficient algorithm for this problem across all three target RMSE. For smaller target RMSE, IEKF is more reliable than TEKI or ETKI, but at a target RMSE of 1.2, TEKI, ETKI or IEKF are comparable and all are slightly more efficient than UKI,

Figure 6(d) illustrates the forcing functions the ensemble methods identify from the statistical data. Since we enforce that all methods reach the same accuracy, all methods generate similar forcing functions, but we note differences in regions where the forcing is large. The reason is that a larger forcing implies more chaotic behavior so that the forcing function is less sensitive to the precise value of the forcing, provided that the forcing is sufficiently large.

4.4 Lorenz'96 dynamics: spatially varying forcing and a neural network parameterization

We now consider L'96 dynamics (dimension $n_z = 100$) under a spatially varying forcing, but for the inversions, we parameterize the forcing function by a neural network – mimicking to some extent ML parameterizations in GCMs (Vishny et al., 2024). Specifically, we estimate the $n_u = 61$ weights and biases of a shallow neural network (one layer, 20 neurons) from statistical data of a L'96 problem with a spatially varying forcing.

4.4.1 Results with an uninformative prior

With the uninformative prior, UKI can only rarely (about 3% of the time) reach the target RMSE (one, 1.1 or 1.2), even though UKI has proven to be efficient in the above problems. The reason is that the uninformative prior distribution leads to poor initial sigma points and, hence, an initial ensemble with a large data misfit. The UKI iteration cannot recover from this poor initial guess and, hence, fails to reach the target RMSE.

The uninformative prior further complicates the loss function landscape, and we do not detect the overall convex loss, corrupted by noise. Instead, we encounter non-convexity at all scales, as illustrated in Figure 7, which shows four slices of the loss function for four neural network weights ($u^{10}, u^{20}, u^{30}, u^{40}$). Here, the true value is determined by fitting a neural network directly to the sinusoidal forcing and we detect that several slices of the loss function are lacking large-scale convex structure.

Figure 8 summarizes the results of our numerical experiments with TEKI, ETKI and IEKF. First, we note that IEKF has a smaller optimal ensemble size than TEKI or ETKI for all three target RMSEs. IEKF, however, struggles to converge and often fails to reach the target RMSE within the maximum number of iterations (120). To improve the stability of IEKF, we used a smaller step size of $\alpha = 0.15$ in all experiments with IEKF (larger step sizes lead to even more failures). For a target RMSE of one, IEKF fails to reach the target RMSE in nearly half of the 100 experiments (Figure 8(d)). The number of failures decreases as the target RMSE increases, but the variation in the number of iterations remains high, even for the larger target RMSEs. In this problem, IEKF is not reliable and computationally more costly than TEKI or ETKI.

TEKI and ETKI are comparable in terms of their optimal ensemble size, number of iterations and number of model runs – although at a target RMSE of one, ETKI fails to reach the target RMSE more often than TEKI and, therefore, is less reliable. We further notice that TEKI and ETKI require a relatively large optimal ensemble size (about 200), but only few iterations (about 20). The reason for the inefficiency of IEKF and UKI are the uninformative prior, which is used very directly by both of these ensemble meth-

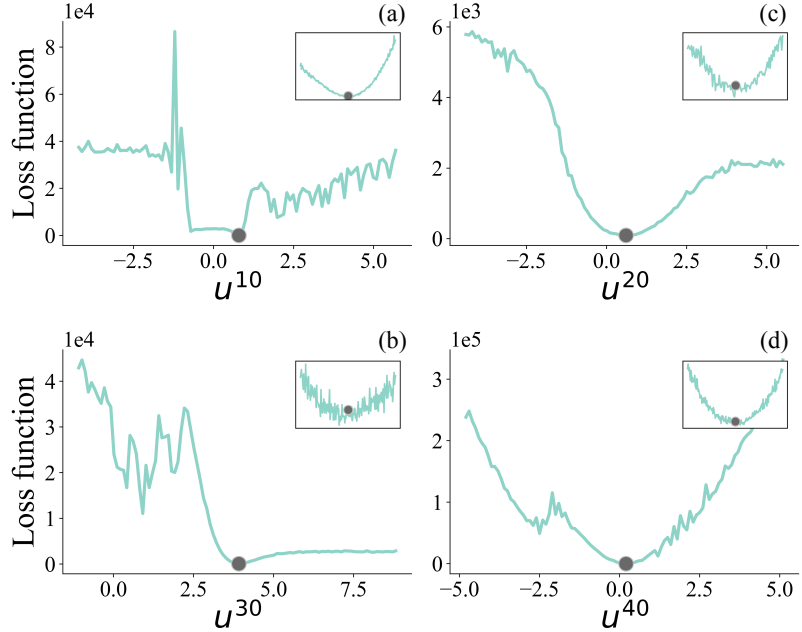


Figure 7. Slices of the loss function defined by the L'96 dynamics with a spatially varying forcing parameterized by a neural network. In each slice, all but one of the weights/biases is fixed at their true values and one weight is varied. The true values of the weights are plotted as dark gray dots. A box in each upper-right corner contains a zoomed in portion of the loss function around the true values. Near the global minimum, we again observe a large-scale convex structure with noise added due to the statistical data.

ods and leads to instability in UKI and a large number of iterations and large variations in the number of iterations for IEKF. TEKI and ETKI make less explicit use of the prior and, therefore, are more robustly applicable in this problem with an uninformative prior.

Figure 8(e) illustrates the forcing functions obtained by the ensemble methods and, as before, we see that all methods produce similar results, albeit at very different computational costs (and provided IEKF indeed reaches the target RMSE). The forcing functions parameterized by the neural networks are smoother than those defined on the grid (Figure 6(d)). The smoother results are expected, because the relatively small neural networks (only 61 weights and biases) with a hyperbolic tangent activation function induce an implicit regularization towards smooth forcing functions.

4.4.2 Results with an informative prior

Results we obtain with L'96 dynamics under a spatially varying forcing with a neural network parameterization and an informative prior distribution are summarized in Figure 9. With the informative prior, all four ensemble methods can reach the target RMSEs reliably, which results in relatively small variations in the number of iterations. Moreover, the informative prior reduces the computational cost of all ensemble methods compared to the experiments with the uninformative prior. The reason is that the optimal ensemble sizes and the required number of iterations of TEKI, ETKI and IEKF are smaller when the prior is informative (compare Figures 8(c) and 9(c)). Moreover, the optimal ensemble size, number of iterations and number of model runs do not vary much from one target RMSE to the next. Variations in the number of iterations and number of model runs, however, decrease as the target RMSE increases.

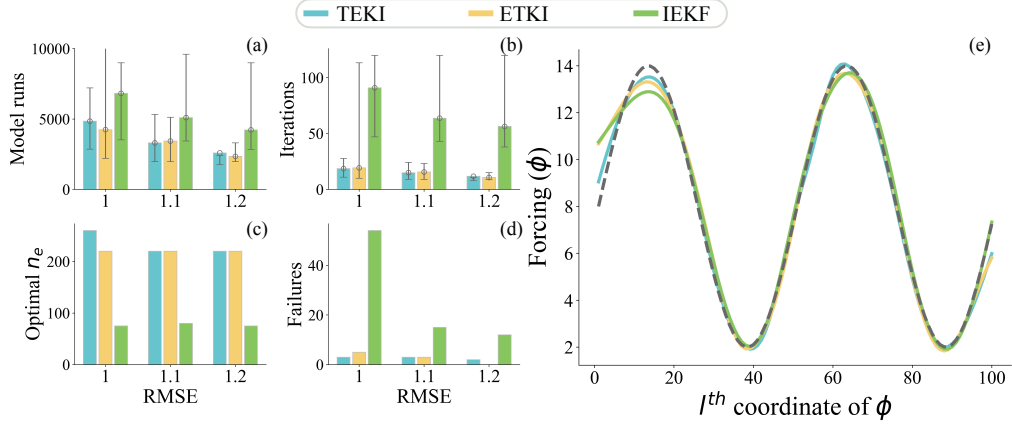


Figure 8. Summary of results for L'96 dynamics under a spatially varying forcing, parameterized by a neural network. (a) Average number of forward model runs required to reach target accuracies of $\text{RMSE} = 1$, $\text{RMSE} = 1.1$, or $\text{RMSE} = 1.2$ (with truncated y axis). (b) Average number of iterations required to reach the target accuracies. The error bars in panels (a) and (b) are derived from the 5th and 95th percentiles. (c) Optimal ensemble sizes for three target accuracies. (d) Total number of ensemble failures (i.e., the RMSE target was not reached within the maximum number of iterations or the algorithm became unstable) over 100 experiments. (e) Spatially varying forcing ϕ_i (black, dashed) and estimated grid-based parameterizations of TEKI (blue), ETKI (yellow), and IEKF (green).

For all three target RMSE s, the optimal ensemble sizes of TEKI, ETKI and IEKF are smaller than the ensemble size of UKI (because the number of unknown parameters is 61, leading to an ensemble size of $n_e = 123$ for UKI). Since UKI requires a larger ensemble size and a larger number of iterations than TEKI, ETKI or IEKF, UKI is not an efficient algorithm for this problem. TEKI, ETKI and IEKF are comparable in their computational cost for all three target RMSE s because their optimal ensemble sizes and number of iterations are comparable. TEKI, however, has the smallest variation in the computational cost across all three target RMSE s and IEKF is characterized by a larger number of model runs (on average and when taking uncertainties into account) than TEKI or ETKI. Thus, even with an informative prior, IEKF can be more computationally expensive than TEKI or ETKI.

Figure 9(d) illustrates the forcing functions obtained by the ensemble methods and, as before, we see that all methods produce similar results. In fact, the forcing estimates for each of the ensemble methods are so similar that the forcing functions have significant overlap. Moreover, the forcing functions recovered with the help of an informative prior most closely resemble the true forcing function, comparing to the grid-based forcing parameterization (Figure 6(d)) or the neural network parameterization in the absence of an informative prior (Figure 8(e)).

4.5 Summary of results obtained with derivative-based optimization

Derivative-based optimization via Levenberg-Marquardt (LM) fails to reach the target RMSE s within the maximum number of iterations for all numerical experiments we considered. The reason is that the noise in the loss produces a landscape full of local minima, therefore optimization methods that derive search directions from locally approximated derivatives get trapped in the local minimum closest to initialization. To illustrate this effect, we compute the normalized difference of the converged LM solution, u_* ,

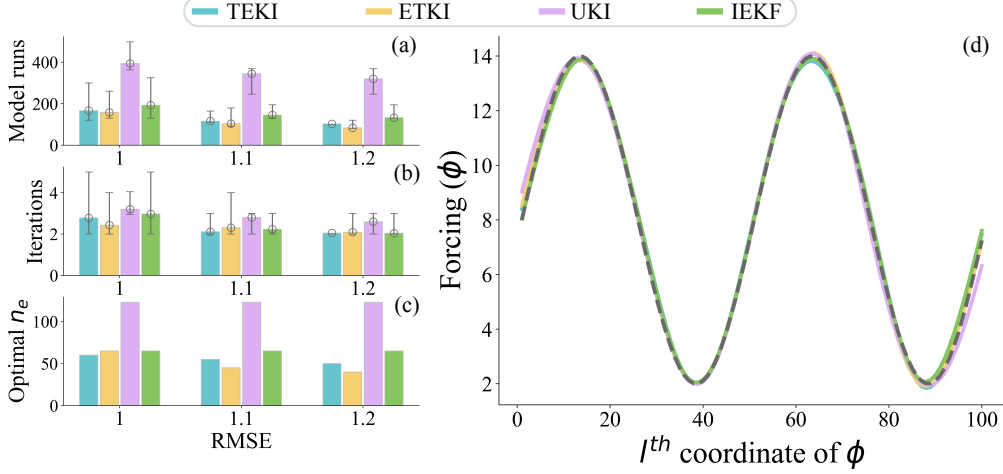


Figure 9. Summary of results for L'96 dynamics under a spatially varying forcing, parameterized by a neural network using an informative prior. (a) Average number of forward model runs required to reach target accuracies of $\text{RMSE} = 1$, $\text{RMSE} = 1.1$, or $\text{RMSE} = 1.2$. (b) Average number of iterations required to reach the target accuracies. The error bars in panels (a) and (b) are derived from the 5th and 95th percentiles. (c) Optimal ensemble sizes for three target accuracies. (d) Spatially varying forcing ϕ_i (black, dashed) and estimated grid-based parameterizations of TEKI (blue), ETKI (yellow), UKI (pink), and IEKF (green).

Dynamics	Parameterizations (u)	Average RMSE	Average Δu
L'63	Model param. ρ, β	9.856	1.316×10^{-1}
L'96	Model param. ϕ	3.269	1.112×10^{-8}
L'96	Grid-based ϕ_i	6.406	3.481×10^{-9}
L'96	Neural Net (weak prior)	180.475	2.728×10^{-8}
L'96	Neural Net (strong prior)	17.815	1.156×10^{-9}

Table 3. Derivative-based optimization via Levenberg-Marquardt (LM) gets trapped in local minima near the starting guess. The result is a small normalized difference Δu in (37) and a large RMSE.

to the starting guess u_0 , defined by

$$\Delta u = \frac{\|u_0 - u_*\|}{\|u_0\|}, \quad (37)$$

where all norms are two-norms. A small normalized difference indicates that LM converged to a nearby local minimum. The averaged normalized difference along with the average RMSE of the LM optimization we performed are summarized in Table 3. We conclude that all test problems we consider here are too noisy to be amenable to derivative-based optimization without further modification.

4.6 Discussion of the results across all five experiments

The EKI race with five different test problems does not reveal a clear winner, in the sense that one EKI variant is most efficient in all five test problems. Our numerical experiments, however, are still informative and support the following guidelines for the use of EKI variants.

1. When the number of unknown parameters n_u is small ($n_u \leq 10$) and if reliable prior information is available in the form of a Gaussian prior, then UKI is efficient in estimating model parameters from time-averaged data. These guidelines are supported by the low-dimensional test problems in Sections 4.1 and 4.2, in which UKI appeared to be the most efficient and most reliable ensemble method. Our higher dimensional test problems in Section 4.3 and 4.4.2 suggest that UKI becomes less efficient than TEKI, ETKI or IEKF, even if the dimension/number of unknowns is $O(10)$. The numerical tests with an uninformative prior in Section 4.4.1 indicate that UKI may be unstable in the absence of reliable prior information.
2. TEKI and ETKI have shown robust performance on all five test problems, indicating that these methods should be considered seriously. In the test problem that is perhaps most similar to GCM calibration (L'96 dynamics, spatially varying forcing, neural network parameterizations), TEKI and ETKI are the most efficient algorithms among the ensemble methods we tried. Moreover, TEKI and ETKI could successfully estimate parameters even if the prior was uninformative, which caused failures in UKI and IEKF.
3. IEKF can be a very efficient method which also provides an approximate uncertainty quantification (whereas TEKI, ETKI or UKI only provide point estimates). IEKF performed well in four of the five test problems, but it failed to be reliable in the absence of a strong prior. If a strong, informative prior is available, IEKF can be a good choice and it can be as efficient as TEKI or ETKI, while also providing an approximate uncertainty quantification.
4. In the higher-dimensional test problems (Sections 4.3, 4.4.1 and 4.4.2), the optimal ensemble sizes of TEKI and ETKI depend on the prior. With an informative prior (4.4.2), TEKI and ETKI can reach the target RMSEs with ensemble sizes less than the number of unknowns, but when the prior is less informative (Section 4.3), these methods may require an ensemble size about two times the number of unknowns. With a very uninformative prior (Section 4.4.1), TEKI and ETKI require an ensemble size larger than three times the number of unknowns. IEKF requires an ensemble size that is larger than the number of unknowns, but does not need the ensemble size to be twice the number of unknowns.
5. The test problems with L'96 dynamics, a spatially varying forcing and a neural network parameterization feature a loss function that is not only noisy, but also non-convex (at all scales). The fact that TEKI, ETKI and, to some extend, IEKF can find a useful solution by optimizing such a complex loss landscape with a weak prior is encouraging for the possible use of these techniques in the context of GCM calibration.
6. The fact that TEKI and ETKI performed similarly on all test problems is not a surprise. Both algorithms solve the same problem in the same way, if we set the ensemble size to infinity. One may therefore view differences in performance between TEKI and ETKI as being largely driven by uncertainties in the initial ensemble or the initial conditions of the dynamics.

TEKI, ETKI and IEKF are in principle scalable to much higher dimensions than we considered here, in the sense that the ensemble size need not scale with the number of unknowns. But, this scaling requires that the covariance estimates within the ensemble iterations are improved via covariance localization or other covariance estimation or sampling error correction methods (Tong & Morzfeld, 2023; Vishny et al., 2024). TEKI and IEKF can be localized via traditional, distance-based localization or by applying covariance estimation and sampling error correction techniques to the covariance and cross-covariance matrices. Localization in transform filters (ETKI) is typically done by considering variables, or sets of variables, independently. Whether or not that is feasible when the unknowns are weights and biases of neural networks (Section 4.4) remains to be investigated, but localized transform filters have proven extremely successful in numerical weather prediction. Thus, whether to use TEKI, IEKF or ETKI for high-dimensional

problems depends on what type of localization strategy is most applicable. Future work will address questions about scalability of TEKI, ETKI and IEKF via localization, covariance estimation and sampling error correction.

5 Summary and conclusions

Ensemble methods are derivative-free optimization and sampling tools that are successfully applied in several nonlinear Earth science applications, e.g., numerical weather prediction, physical oceanography and reservoir engineering. We consider the use of ensemble methods in the context of climate science problems, specifically global climate model (GCM) calibration, where climate model parameters or parameterizations are estimated from time-averaged data. The loss functions that arise in this context are noisy and can be non-convex. Ensemble methods can handle such complex loss landscapes because (i) the use of an ensemble instead of a derivative smooths over the noise in the loss function; and (ii) ensemble methods locally linearize statistically, but do not require globally linear models, Gaussian likelihoods or priors, or even, as we have shown, global convexity of the loss function.

Given that there are many variants of ensemble methods in the literature, we have carefully investigated the question: “*Which ensemble method variant is most efficient for estimating model parameters from time-averaged data generated by chaotic dynamics?*” because it is relevant for GCM calibration. We have designed a set of systematic numerical experiments that allow us to investigate several aspects of the GCM calibration problem: scalability of ensemble methods with the number of unknown parameters, influence of the prior distribution on the numerical efficiency of an ensemble method, and robustness to complex, noisy, non-convex loss landscapes. The numerical experiments are systematic in that we chose an optimal ensemble size to maximize computational efficiency of each method, define iteration exit criteria to ensure a desired target accuracy, and construct meaningful observation error covariance matrices for time-averaged data. Such systematic numerical experiments are computationally very expensive to perform with GCMs, even at low resolution. We designed forward models based on well-known chaotic Lorenz-type dynamics, and considered various configurations of estimating model parameters or model parameterizations.

Being mindful of simplifications implied by the Lorenz-type dynamics, we argued that we can still extract practically useful guidelines from our experiments. Specifically, our recommendations are that UKI is an efficient option if the number of unknowns is small ($n_u \leq 10$); IEKF is an efficient option if the prior is informative; TEKI and ETKI are the most robust methods, but with a strong prior, IEKF can be computationally more efficient. Given the diversity of methods, and consideration of the problem setup, one will likely find a good candidate algorithm. Moreover, all methods are appropriate in the setting of calibration to statistical data, where derivative-based methods demonstrably fail to produce useful solutions. Though not a deep or exhaustive comparison, in the recent age of building auto-differentiable climate model components, this highlights a potential problem that such derivatives may not be usable for parameter calibration to observable statistics. To improve the existing ensemble methods, research in areas such as removing tight constraints on UKI with high dimensional inputs and implementing ETKI with high dimensional inputs is welcome.

Our numerical experiments do not consider performance enhancements of ensemble methods via covariance localization, inflation, acceleration, and adaptive timestepping though these techniques are critical to the successful application of ensemble methods in high-dimensional problems. Our overall framework of performing systematic numerical experiments, however, largely applies to testing such enhancements: We could, for example, re-run the experiments with L'96 dynamics and spatially varying forcing in higher dimensions and with localization and inflation - such experiments are left for

follow-up work. Similarly, it is possible to adjust our framework of numerical experiments to ensemble methods that approximate Bayesian posterior distributions (rather than the optimization methods we focused on). Many existing methods require additional tuning parameters, and will require new metrics to measure the difference between exact and approximate posterior distributions.

Our relatively simple numerical test problems underline the challenges of hybridizing GCMs with the modern ML techniques, such as introducing data-driven components. The loss landscape is always noisy due to the statistical data, but we find neural network parameterizations may induce further complications due to the difficulty of defining reliable (Gaussian) priors that lead to non-convex loss landscapes, and inhibits some ensemble methods from reliable convergence. We consider offline-online approaches for the construction of priors for neural network weights, but more work is needed to promote good guidelines. Our tests suggest that ensemble methods, in particular TEKI and ETKI, can handle such complex loss functions, with and without reliable prior information, and, therefore, remain a promising tool for hybrid GCM calibration.

Open Research Section

The code and data used for this manuscript will be provided upon acceptance. The code and data will be uploaded to both Github and Zenodo.

Acknowledgments

RG and MM are supported by the US Office of Naval Research (ONR) (grant N00014-21-1-2309). ORAD and TS are supported by Schmidt Sciences, LLC, the U.S. National Science Foundation (grant AGS-1835860), and ONR (grant N00014-23-16161-2654).

References

- Al-Ghattas, O., & Sanz-Alonso, D. (2023, 12). Non-asymptotic analysis of ensemble Kalman updates: effective dimension and localization. *Information and Inference: A Journal of the IMA*, 13(1), iaad043. Retrieved from <https://doi.org/10.1093/imaiia/iaad043> doi: 10.1093/imaiia/iaad043
- Arbel, J., Pitas, K., Vladimirova, M., & Fortuin, V. (2023). *A primer on Bayesian neural networks: Review and debates*. Retrieved from <https://arxiv.org/abs/2309.16314>
- Bieli, M., Dunbar, O. R. A., de Jong, E. K., Jaruga, A., Schneider, T., & Bischoff, T. (2022). An efficient Bayesian approach to learning droplet collision kernels: Proof of concept using “cloudy,” a new n-moment bulk microphysics scheme. *Journal of Advances in Modeling Earth Systems*, 14(8), e2022MS002994. Retrieved from <https://agupubs.onlinelibrary.wiley.com/doi/abs/10.1029/2022MS002994> doi: <https://doi.org/10.1029/2022MS002994>
- Bishop, C. H., Etherton, B. J., & Majumdar, S. J. (2001). Adaptive sampling with the ensemble transform Kalman filter. Part I: Theoretical aspects. *Monthly Weather Review*, 129(3), 420 - 436. Retrieved from https://journals.ametsoc.org/view/journals/mwre/129/3/1520-0493_2001_129_0420_aswtet_2.0.co_2.xml doi: 10.1175/1520-0493(2001)129<0420:ASWTET>2.0.CO;2
- Bocquet, M., & Sakov, P. (2014). An iterative ensemble Kalman smoother. *Quarterly Journal of the Royal Meteorological Society*, 140(682), 1521-1535. Retrieved from <https://rmets.onlinelibrary.wiley.com/doi/abs/10.1002/qj.2236> doi: <https://doi.org/10.1002/qj.2236>
- Carrillo, J. A., Hoffmann, F., Stuart, A. M., & Vaes, U. (2024). The mean-field ensemble Kalman filter: Near-gaussian setting. *SIAM Journal on Numerical*

- Analysis*, 62(6), 2549-2587. doi: 10.1137/24M1628207
- Chada, N. K., Chen, Y., & Sanz-Alonso, D. (2021). Iterative ensemble Kalman methods: A unified perspective with some new variants. *Foundations of Data Science*, 3(3), 331-369. Retrieved from <https://www.aims sciences.org/article/id/dbcb5d0f-605d-4752-a353-20f42771f6f3> doi: 10.3934/fods.2021011
- Chada, N. K., Stuart, A. M., & Tong, X. T. (2020). Tikhonov regularization within ensemble Kalman inversion. *SIAM Journal on Numerical Analysis*, 58(2), 1263-1294. Retrieved from <https://doi.org/10.1137/19M1242331> doi: 10.1137/19M1242331
- Chada, N. K., & Tong, X. T. (2019). Convergence acceleration of ensemble Kalman inversion in nonlinear settings. *Mathematics of Computation*, 91(335), 1247-1280. Retrieved from <https://api.semanticscholar.org/CorpusID:207880575>
- Chen, Y., & Oliver, D. S. (2012). Ensemble randomized maximum likelihood method as an iterative ensemble smoother. *Mathematical Geosciences*, 44, 1-26.
- Chen, Y., & Oliver, D. S. (2013). Levenberg–Marquardt forms of the iterative ensemble smoother for efficient history matching and uncertainty quantification. *Computational Geosciences*, 17(4), 689–703. Retrieved from <https://doi.org/10.1007/s10596-013-9351-5> doi: 10.1007/s10596-013-9351-5
- Christopoulos, C., Lopez-Gomez, I., Beucler, T., Cohen, Y., Kawczynski, C., Dunbar, O. R. A., & Schneider, T. (2024). Online learning of entrainment closures in a hybrid machine learning parameterization. *J. Adv. Model. Earth Sys.*, 16, e2024MS004485.
- Cleary, E., Garbuno-Inigo, A., Lan, S., Schneider, T., & Stuart, A. M. (2021). Calibrate, emulate, sample. *Journal of Computational Physics*, 424, 109716. Retrieved from <https://www.sciencedirect.com/science/article/pii/S0021999120304903> doi: <https://doi.org/10.1016/j.jcp.2020.109716>
- Deck, K., Braghieri, R. K., Renchon, A. A., Sloan, J., Bozzola, G., Speer, E., ... Schneider, T. (2025). ClimaLand: A land surface model designed to enable data-driven parameterizations. *J. Adv. Model. Earth Sys.*, *in review*.
- Dunbar, O. R. A., Garbuno-Inigo, A., Schneider, T., & Stuart, A. M. (2021). Calibration and Uncertainty Quantification of Convective Parameters in an Idealized GCM. *Journal of Advances in Modeling Earth Systems*, 13(9), e2020MS002454. Retrieved from <https://agupubs.onlinelibrary.wiley.com/doi/abs/10.1029/2020MS002454> doi: <https://doi.org/10.1029/2020MS002454>
- Dunbar, O. R. A., Lopez-Gomez, I., Garbuno-Iñigo, A., Huang, D. Z., Bach, E., & long Wu, J. (2022). EnsembleKalmanprocesses.jl: Derivative-free ensemble-based model calibration. *Journal of Open Source Software*, 7(80), 4869. Retrieved from <https://doi.org/10.21105/joss.04869> doi: 10.21105/joss.04869
- Emerick, A. A., & Reynolds, A. C. (2012). History matching time-lapse seismic data using the ensemble Kalman filter with multiple data assimilations. *Computational Geosciences*, 16(3), 639–659. Retrieved from <https://doi.org/10.1007/s10596-012-9275-5> doi: 10.1007/s10596-012-9275-5
- Emerick, A. A., & Reynolds, A. C. (2013). Ensemble smoother with multiple data assimilation. *Computers & Geosciences*, 55, 3-15. Retrieved from <https://www.sciencedirect.com/science/article/pii/S0098300412000994> (Ensemble Kalman filter for data assimilation) doi: <https://doi.org/10.1016/j.cageo.2012.03.011>
- Evensen, G. (1994). Sequential data assimilation with a nonlinear quasi-geostrophic model using Monte Carlo methods to forecast error statistics. *Journal of Geophysical Research*, 99, 10143-10162. Retrieved from <https://api.semanticscholar.org/CorpusID:16213443>

- Evensen, G. (2009). *Data assimilation. the ensemble Kalman filter* (Second ed.). Springer. doi: 10.1007/978-3-642-03711-5
- Evensen, G. (2018). Analysis of iterative ensemble smoothers for solving inverse problems. *Computational Geosciences*, 22(3), 885–908. Retrieved from <https://doi.org/10.1007/s10596-018-9731-y> doi: 10.1007/s10596-018-9731-y
- Garbuno-Inigo, A., Hoffmann, F., Li, W., & Stuart, A. M. (2020). Interacting langevin diffusions: Gradient structure and ensemble Kalman sampler. *SIAM Journal on Applied Dynamical Systems*, 19(1), 412-441. doi: 10.1137/19M1251655
- Garbuno-Inigo, A., Nüsken, N., & Reich, S. (2020). Affine invariant interacting langevin dynamics for bayesian inference. *SIAM Journal on Applied Dynamical Systems*, 19(3), 1633–1658.
- Gu, Y., & Oliver, D. S. (2007, 12). An iterative ensemble Kalman filter for multi-phase fluid flow data assimilation. *Society of Petroleum Engineers (SPE) Journal*, 12(04), 438-446. Retrieved from <https://doi.org/10.2118/108438-PA> doi: 10.2118/108438-PA
- Huang, D. Z., Huang, J., Reich, S., & Stuart, A. M. (2022, oct). Efficient derivative-free Bayesian inference for large-scale inverse problems. *Inverse Problems*, 38(12), 125006. Retrieved from <https://dx.doi.org/10.1088/1361-6420/ac99fa> doi: 10.1088/1361-6420/ac99fa
- Huang, D. Z., Schneider, T., & Stuart, A. M. (2022). Iterated Kalman methodology for inverse problems. *Journal of Computational Physics*, 463, 111262.
- Iglesias, M. A., Law, K. J. H., & Stuart, A. M. (2013, mar). Ensemble Kalman methods for inverse problems. *Inverse Problems*, 29(4), 045001. Retrieved from <https://dx.doi.org/10.1088/0266-5611/29/4/045001> doi: 10.1088/0266-5611/29/4/045001
- Julier, S. J., & Uhlmann, J. K. (1997). New extension of the Kalman filter to non-linear systems. In I. Kadar (Ed.), *Signal processing, sensor fusion, and target recognition vi* (Vol. 3068, pp. 182 – 193). SPIE. Retrieved from <https://doi.org/10.1117/12.280797> doi: 10.1117/12.280797
- Kozyrskiy, B., Milios, D., & Filippone, M. (2023). Imposing functional priors on Bayesian neural networks. In *Icpram 2023, 12th international conference on pattern recognition applications and methods*.
- Ledoit, O., & Wolf, M. (2022). The power of (non-) linear shrinking: A review and guide to covariance matrix estimation. *Journal of Financial Econometrics*, 20(1), 187–218.
- Levenberg, K. (1944). A method for the solution of certain non-linear problems in least squares. *Quarterly of Applied Mathematics*, 2(2), 164–168. Retrieved 2025-09-19, from <http://www.jstor.org/stable/43633451>
- Lopez-Gomez, I., Christopoulos, C., Langeland Ervik, H. L., Dunbar, O. R. A., Cohen, Y., & Schneider, T. (2022). Training physics-based machine-learning parameterizations with gradient-free ensemble kalman methods. *Journal of Advances in Modeling Earth Systems*, 14(8), e2022MS003105. Retrieved from <https://agupubs.onlinelibrary.wiley.com/doi/abs/10.1029/2022MS003105> doi: <https://doi.org/10.1029/2022MS003105>
- Lorenz, E. N. (1963). Deterministic nonperiodic flow. *Journal of Atmospheric Sciences*, 20(2), 130 - 141. Retrieved from https://journals.ametsoc.org/view/journals/atsc/20/2/1520-0469_1963_020_0130_dnf_2_0_co_2.xml doi: 10.1175/1520-0469(1963)020(0130:DNF)2.0.CO;2
- Lorenz, E. N. (1995, 1995). Predictability: a problem partly solved. *Proc. ECMWF Seminar on predictability*, 1, 1-18.
- Marquardt, D. W. (1963). An algorithm for least-squares estimation of nonlinear parameters. *Journal of the Society for Industrial and Applied Mathematics*, 11(2), 431-441. Retrieved from <https://doi.org/10.1137/0111030> doi: 10

- .1137/0111030
- Moré, J. J., & Wild, S. M. (2009). Benchmarking derivative-free optimization algorithms. *SIAM Journal on Optimization*, 20(1), 172-191. Retrieved from <https://doi.org/10.1137/080724083> doi: 10.1137/080724083
- Nocedal, J., & Wright, S. (2006). *Numerical optimization* (Second ed.). Springer.
- Pahlavan, H. A., Hassanzadeh, P., & Alexander, M. J. (2024). Explainable offline-online training of neural networks for parameterizations: A 1D gravity wave-QBO testbed in the small-data regime. *Geophysical Research Letters*, 51(2), e2023GL106324.
- Santitissadeekorn, N., & Jones, C. (2015). Two-stage filtering for joint state-parameter estimation. *Monthly Weather Review*, 143(6), 2028–2042.
- Schillings, C., & Stuart, A. (2017, 02). Analysis of the ensemble Kalman filter for inverse problems. *SIAM Journal on Numerical Analysis*, 55(3), 1264–1290. doi: 10.1137/16M105959X
- Schillings, C., & Stuart, A. M. (2018). Convergence analysis of ensemble Kalman inversion: the linear, noisy case. *Applicable Analysis: An International Journal*, 97(1), 107–123. (Funding by Engineering and Physical Sciences Research Council (EPSRC)) doi: 10.1080/00036811.2017.1386784
- Schneider, T., Behera, S., Boccaletti, G., Deser, C., Emanuel, K., Ferrari, R., ... Yamagata, T. (2023, 09). Harnessing AI and computing to advance climate modelling and prediction. *Nature Climate Change*, 13, 887-889. doi: 10.1038/s41558-023-01769-3
- Schneider, T., Lan, S., Stuart, A., & Teixeira, J. (2017). Earth system modeling 2.0: A blueprint for models that learn from observations and targeted high-resolution simulations. *Geophysical Research Letters*, 44(24), 12,396-12,417. Retrieved from <https://agupubs.onlinelibrary.wiley.com/doi/abs/10.1002/2017GL076101> doi: <https://doi.org/10.1002/2017GL076101>
- Schneider, T., Leung, L. R., & Wills, R. C. J. (2024). Opinion: Optimizing climate models with process-knowledge, resolution, and AI. *EGUsphere*, 2024, 1–26. Retrieved from <https://egusphere.copernicus.org/preprints/2024/egusphere-2024-20/> doi: 10.5194/egusphere-2024-20
- Schneider, T., Stuart, A., & Wu, J. (2020, 04). Learning stochastic closures using ensemble Kalman inversion. *Transactions of Mathematics and Its Applications*, 5(1). doi: 10.1093/imatrnab/003
- Schneider, T., Teixeira, J., Bretherton, C. S., Brant, F., Pressel, K. G., Schär, C., & Siebesma, A. P. (2017). Climate goals and computing the future of clouds. *Nature Climate Change*, 7(1), 3–5.
- Tippett, M. K., Anderson, J. L., Bishop, C. H., Hamill, T. M., & Whitaker, J. S. (2003). Ensemble square root filters. *Monthly Weather Review*, 131(7), 1485 - 1490. doi: 10.1175/1520-0493(2003)131<1485:ESRF>2.0.CO;2
- Tong, X. T., & Morzfeld, M. (2023, apr). Localized ensemble Kalman inversion. *Inverse Problems*, 39(6), 064002. Retrieved from <https://dx.doi.org/10.1088/1361-6420/accb08> doi: 10.1088/1361-6420/accb08
- Vishny, D., Morzfeld, M., Gwirtz, K., Bach, E., Dunbar, O. R. A., & Hodys, D. (2024). High-dimensional covariance estimation from a small number of samples. *Journal of Advances in Modeling Earth Systems*, 16(9), e2024MS004417. Retrieved from <https://agupubs.onlinelibrary.wiley.com/doi/abs/10.1029/2024MS004417> doi: <https://doi.org/10.1029/2024MS004417>
- Wan, E., & Van Der Merwe, R. (2000). The unscented Kalman filter for nonlinear estimation. In *Proceedings of the ieee 2000 adaptive systems for signal processing, communications, and control symposium (cat. no.00ex373)* (p. 153-158). doi: 10.1109/ASSPCC.2000.882463